ACS APPLIED MATERIALS & INTERFACES

Research Article

www.acsami.org

Corrosion-Controlling and Osteo-Compatible Mg Ion-Integrated Phytic Acid (Mg-PA) Coating on Magnesium Substrate for Biodegradable Implants Application

Yingqi Chen,[†] Sheng Zhao,[†] Bo Liu,[†] Meiyun Chen,[†] Jinlong Mao,[†] Hairuo He,[‡] Yuancong Zhao,[†] Nan Huang,[†] and Guojiang Wan*

[†]Key Laboratory of Advanced Technologies of Materials, Ministry of Education, College of Materials Science and Engineering, Southwest Jiaotong University, Chengdu 610031, China

[‡]Department of Chemistry, Hollins University, Roanoke, Virginia 24020-1707, United States

ABSTRACT: Biodegradable, a new revolutionary concept, is shaping the future design of biomedical implants that need to serve only as a temporary scaffold. Magnesium appears to be the most promising biodegradable metal, but challenges remain in its corrosion-controlling and uncertain biocompatibility. In this work, we employ chemical conversion and alternating dip-coating methods to anchor and deposit an Mg ion-integrated phytic acid (Mg-PA) coating on Mg, which is supposed to function both corrosion-controlling and osteo-compatible. It was ascertained that PA molecules were covalently immobilized on a chemically converted $Mg(OH)_2$ base layer, and more PA molecules were deposited subsequently via chelating reactions with the help of additive Mg ions. The covalent immobilization and the Mg ion-supported chelating deposition contribute to a dense and homogeneous protective Mg-PA coating, which guarantees an improved corrosion resistance as well as a reduced degradation rate. Moreover, the Mg-PA coating performed osteo-compatible to promote not only bioactivity of bonelike apatite precipitation, but also induced osteoblast cells adhesion and proliferation. This is ascribed to its nature of PA molecule and the biocompatible Mg ion, both of which mimic partly the compositional structure of bone. Our magnesium ion-integrated PA-coated Mg might bode well for the future of biodegradable bone implant application.

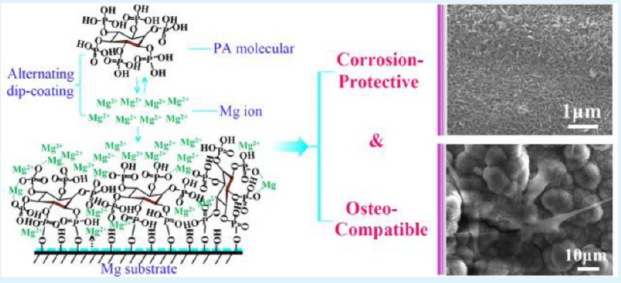

KEYWORDS: *biodegradable metals, bone implants, magnesium, osteo-biocompatibility, phytic acid, corrosion*

1. INTRODUCTION

Metallic materials have found already wide applications in biomedical devices like bone implants, but the choice remains still limited because they provide only insufficient biocompatibility.[1] Common examples in clinical application are 316L stainless steel, titanium, cobalt, tantalum and their alloys. Intuitively, they are selected as corrosion-resistant as possible to maintain the integrity of implants as well as prevent the release of toxic ions. Nevertheless, their permanent presence in the body will inevitably elicit side-effects because actually none of materials explored so far is satisfactorily biocompatible.[2] The adverse effects include cytotoxicity, thrombogenicity, complement system activation, chronic inflammation, and foreign body giant cells formation, among others and their complications.[3] Moreover, long-term contact with foreign material will usually delay the target lesion healing process, produce a mechanical mismatch between surrounding tissues and biomaterials, preclude second surgical procedure, and exclude some advanced diagnostic techniques. Hence, a paradigm-shift is toward biodegradable materials that fulfill the mission that the implants just do a transient scaffolding job and then disappear to avoid the late adverse bioreactions completely.[1−3]

One ideal biodegradable material is desired to, at least, (1) serve well as a temporary mechanical scaffold,[4] (2) degrade at a suitably controlled rate, and (3) perform biocompatibly/-functionally to help lesion healing.[4−7] Magnesium appears to be the most promising metal for biodegradable applications because of its ease of corrosion, good mechanical properties, and unquestionable biosafety.[4] For instance, Mg is an extremely active metal, rendering it capable of easy biocorrosion/degradation; it has an elastic modulus much closer to cortical bone than other metals, which is beneficial for reducing the risk of stress shielding in bone implant applications; Mg ion is the fourth most abundant cation in the human body,[4,7] which exerts various basic biofunctionalities and has a safe metabolism what makes it well-tolerated; Mg is also hypothrombogenic because of its high electronegativity based on electrochemical mechanism of biomaterials-associated thrombosis.[7] However, the biggest challenge for medical applications is its too rapid corrosion.[8−11] The fast corrosion leads usually to premature

Received: January 31, 2014
Accepted: November 3, 2014
Published: November 3, 2014

Scheme 1. Scheme of Establishment of a Covalently Immobilized Mg Ion-Integrated Phytic Acid Coating on Mg Surface

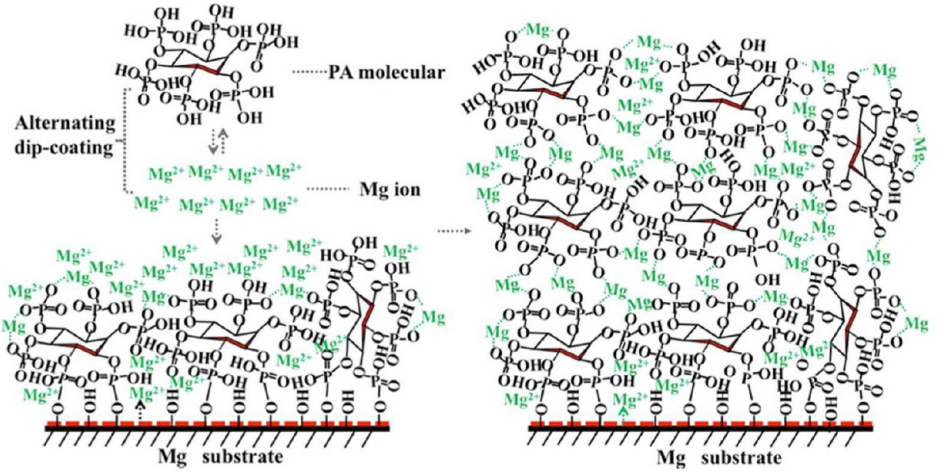

mechanical failure of the implants,[10] byproducts of hydrogen gas cavity and locally increased pH value, both of which irritate harmfully the surrounding tissues.[10,12] Equally, another concern arises from uncertain biocompatibility of such new biometal with dynamic degrading surface.[10]

There recently have been tremendous efforts dedicated to modify Mg and its alloys for biodegradable application. Their strategies fall into two general categories, namely bulk treatment and surface modification. Bulk treatment typically includes alloying, heavy plastic deformation, glass formation and rapid solidification.[3,13−18] Surface modification usually encompasses two subtypes, i.e., chemical conversion and deposition,[19−30] and the methods include plasma electrolytic oxidation,[20,21] phosphate treatment,[22] alkaline heat treatment,[23] microarc oxidation coating,[10,24] anodization treatment,[25] chemical conversion coating,[26] organic coating,[27,28] to name just a few. Major attention so far has been focused on biocorrosion control, while little has been done currently to tackle both biocorrosion/-degradation and biocompatibility simultaneously. Take internal fixation devices (pins, screws, staples, plates, and suture anchors) for bone fracture as an example, both well-controlled biodegradability and good osteo-compatibility (osteo-synthesis, -integrity, -conductivity, and -inductivity) are highly desirable in clinical practice.[29,31] So, the dual-task performance design is of necessity but it is still challenging and has been rarely reported.

Herein, we demonstrate a surface modification strategy of building a ligand-like Mg ion-integrated phytic acid (Mg-PA) coating onto an Mg substrate, by utilizing in situ chemical conversion in conjunction with alternating dip-coating methods. The aim is to form a covalently immobilized surface coating on Mg, with both corrosion-protective and osteo-biocompatible functionalities. Phytic acid ($C_6H_{18}O_{24}P_6$, PA), a natural and nontoxic organic macromolecule, commonly distilled from grains, is frequently applied as one kind of corrosion inhibitor. PA behaves relatively biocompatible and degradable/absorbable in human body.[32] In addition, PA consists of 24 oxygen atoms, 12 hydroxyl groups and 6 phosphate carboxyl groups,[33] and this renders a powerful capability of chelating with many metal ions. Our previous work demonstrated an effective PA deposition on Mg with help of alkaline pretreatment to covalently anchor PA molecules.[34] In the present work, based on this interfacial immobilization, we implement a chemical strategy of combining additional magnesium ions with PA to form a chelate complex for improving the integrity of coating. An alternating dip-coating process was designed to create a more integrated multilayer system by adding Mg ions and PA molecules in an interactive way. Likewise, the Mg chelated PA is assumed to be osteo-compatible in that on one hand PA per se might be able to induce bioactivity of CaP precipitation for bone growth because of their compositional similarity, and on the other hand the incorporated magnesium ion might offer potentially good osteo-compatibility as it is abundant in bone tissue. We investigate herein the electrochemical corrosion and immersion biodegradation behavior, assess the in vitro osteo-compatibility as well as fathom the mechanism therein of this new ligand-like Mg-PA-coated Mg for biodegradable bone implant application.

2. MATERIALS AND METHODS

2.1. Sample Preparation. Commercially purchased pure magnesium disks (purity 99.9%) with a dimension of 10 mm and thickness of 1.5 mm were used as substrates. The substrates were mechanically ground with SiC paper of successively finer roughness down to 2000 grit. Afterward, the samples were ultrasonically cleaned in acetone, alcohol, distilled water and were washed with alkaline solution (10 g/L NaOH, 20g/L $NaCO_3$, 10 g/L triethanolamine) at 60 °C for 10 min. To remove the surface contaminates, we immersed the pretreated samples in an acid solution (22 g/L HNO_3, 150 g/L $MgNO_3$, 300 g/L ethanol) for 30 s at room temperature.[35] The samples were finally cleaned in distilled water and dried in the oven.

2.2. Magnesium Ion-Integrated Phytic Acid Deposition. Prior to deposition of phytic acid, in situ chemical conversion was conducted by immersion of cleaned samples in 3 M NaOH solution for 24 h at 60 °C to obtain a $Mg(OH)_2$ passivation layer. The alkaline-pretreated samples were subsequently washed with distilled water (5 min ×3 times), then dried in the oven. An alternating dip-coating process was executed to deposit an Mg-ion integrated PA coating. Briefly, the alkaline pretreated Mg was immersed in the solution of 5 mg of PA (analytical grade, purity = 99%, Aladdin Chemistry Co. Ltd.) per 1 mL distilled water (pH 5, adjusted by NaOH) at 60 °C for 40 min to realize covalently interfacial immobilization of PA unto the $Mg(OH)_2$ layer; After that, the PA-modified samples were washed with distilled water to remove the PA that had not reacted with the alkaline pretreated Mg, and dried in the oven subsequently. Then, the PA-modified samples were immersed in $MgSO_4$ (analytical grade, purity ≥90%, Jin Shan Hua Shi Co. Ltd.) solution (0.5 mol/L) at 25 °C for 20 min to allow Mg ion incorporation into PA layer. The Mg ions containing PA modified samples were then immersed in above-mentioned PA solution to achieve chelating reactions between PA molecules and Mg ions. The process was alternatively conducted for 5

cycles as the optimal condition. The magnesium ion-integrated PA coated Mg is referred to as Mg-OH@Mg-PA. Scheme 1 portrays schematically one cycle process of Mg ion-integrated PA deposition. Direct PA-deposited Mg (without immersion in $MgSO_4$ solution, for the same deposition time), referred to as Mg-OH@PA, and pure Mg were used as controls for comparison.

2.3. Characterization. The surface morphology was observed by optical microscopy (MM6, Leitz Company), atomic force microscope (AFM, SPI 3800, NSK Inc.; in contacting mode with the scanning range of 10 μm × 10 μm), and field-emission scanning electron microscopy (FESEM, JSM-7401F, JEOL, Japan). The chemical structure characteristic was detected by Fourier transform infrared spectroscopy (FT-IR, Nicolet 5700). The surface chemical composition and bonding states were determined by X-ray photoelectron spectroscopy (XPS, XSAM800, Kratos Ltd., UK), which was equipped with a monochromatic Al Kα (1486.6 eV) X-ray source operate at 12 kV × 15 mA at a pressure of 2×10^{-7} Pa. The C 1s peak (binding energy 284.8 eV) was used as calibration reference. The peaks were fitted using Xpspeak 4.1 to analyze the high resolution spectrum. The phase structure of samples was characterized by X-ray diffraction (XRD, Philip X'Pert) using a CuK radiation with a glancing angle of 2°. The XRD data were obtained in a 2θ range of 20−40° at a step size of 0.25°.

Static (sessile drop) contact angles of water and diiodomethane were measured by a contact angle apparatus DSA100 (Krüss, Hamburg, Germany). A droplet of deionized water was added to the surface of the samples, and the contact angle was read through a horizontal microscope (at 25 °C and 60% relative humidity). For each sample, the mean value of the contact angles was calculated from at least three individual measurements taken at different sites on the samples. The number of the samples used for statistical analysis is no less than four. The surface energy of the samples was calculated by the method described by Owens and Wendt[36] with the contact angle data of water and diiodomethane.

2.4. Electrochemical Corrosion Test. The electrochemical corrosion experiments were conducted on an electrochemical workstation (IM6, Zahner, Germany). A conventional three-electrode arrangement was employed, namely a saturated calomel electrode (SCE) as reference electrode, a platinum foil (1.5 × 1.5 cm^{-1}) as counter-electrode and the disc samples as working electrode. All the tested samples were connected to a copper wire and then were sealed with silicon rubber, exposing 0.79 cm^2 area of research surface. The electrolyte was phosphate buffered saline (PBS) at 37 ± 0.5 °C. Prior to the potentiodynamic polarization (PDP) test, all the samples were stabilized in PBS for 30 min. The PDP test was performed at a scanning rate of 1 mV/s. The corrosion potentials E_{corr} and current density I_{corr} were determined by the Tafel method through linear extrapolation of active polarization zone (in cathodic polarization section when the over potential was about 50 mV less than free corrosion potential).[37]

Electrochemical impedance spectroscopy (EIS) measurements were conducted on the same electrochemical workstation as the PDP test; the electrolyte cell was confined in a faraday cage to avoid disturbances. The samples were stabilized in PBS for 30 min prior to testing. The data were recorded from 200 kHz to 10 mHz with a 10 mV sinusoidal perturbing signal at the open-circuit potential. The EIS data analysis software ZsimDemo was used to analyze the impedance data.

2.5. Immersion Degradation Test. The degradation behavior of the specimens was investigated by immersion test in PBS. The volume of evolved hydrogen and change of pH were gauged as indicators for estimation of the Mg degradation rate. The number of the samples used for statistical count is no fewer than four. All of the tests were performed at least two times.

2.5.1. Volume of Hydrogen Evolution. The epoxy resin sealed specimens (four for each kind sample) with a test area of 0.79 cm^2 were put in PBS (300 mL, adjusted to 7.4 ± 0.2) at 37 ± 0.5 °C. The hydrogen gas was collected by an eudiometer.[38] The surface morphology of the specimens after the immersion test (hydrogen evolution) was observed by SEM.

2.5.2. Change of pH. The specimens were sealed with epoxy resin with a test area of 0.79 cm^2, and then immersed in PBS (40 mL) at 37 ± 0.5 °C. The pH value was measured by a STARTER 3100 pH meter (OHAUS, USA).

2.6. In Vitro Osteo-Compatibility Performance. *2.6.1. In Vitro Bioactivity Evaluation of Calcium Phosphate Precipitation.* A supersaturated calcium phosphate solution was prepared with a mixture of 2.32 mmol/L $NH_4H_2PO_4$, 3.87 mmol/L $CaCl_2$, 150 mmol/L NaCl and 50 mmol/L Tris (Tri (Hydroxymethyl) aminomethane) in deionized water at room temperature.[39] The ion concentration ratio of Ca/P was 1.67 in the used mixture, which is close to that of hydroxyapatite (HA).[31] The disc samples were immersed horizontally into the beakers for 10 s and then were pulled out straightly. After that, the immersed samples dried in the oven (37 °C). After 10 times of "immersed-dried" treatment, the specimens were washed with distilled water. Afterward, each sample was immersed into 50 mL of supersaturated solution for 10 h at 37 ± 0.5 °C. Then specimens were washed with distilled water, dried in the oven, and ready for observation.

2.6.2. Primary Mouse Osteoblasts Compatibility. Becase of the limitation of current in vitro methodology on degrading Mg-based metals (the excessive Mg ions, increased pH value and hydrogen gas will change the culture medium and influence the detection accuracy),[40,41] two experimental schemes were adopted to evaluate respectively the short-time and an extended-time osteoblastic cytocompatibility of the coating. For short-time (2 and 6 h) evaluation, cells were directly seeded (2×10^4 cells/mL) on the coatings on Mg substrate. While for longer-time (1, 3, 5, 7, 14, 21 days) evaluation, cells were seeded (2×10^4 cells/mL) on the Mg-PA coating produced on a Ti-foil (size, 10 mm × 10 mm; purchased from Baoti group Company, China), which is stable in the medium to allow for extended testing periods. In order to replicate the counterpart of coatings on the Mg substrate, the Ti substrate was pretreated and coated in parallel with the Mg substrate strictly according to the same protocol as mentioned above. Ti itself is known as one of the best reference biomaterials in terms of osteo-compatibility.

Primary rat osteoblasts were isolated from the newborn rat's cranium (Vista, ca. 10 days old, suckling rat) according to the reference[42] and cultured in the Minimum Essential Medium Alpha (a-MEM, Corning cellgro@, USA) supplemented with 10% fetal bovine serum (FBS, Hyclone Company). Prior to cells compatibility assessment on the specimens, the primary osteoblasts were at first cultured in a humidified incubator under 5% CO_2 at 37 °C. Then, the osteoblasts were digested by the trypsin, and the cells were seeded on the surface of the samples at a density of 2×10^4 cells/ml by taking the cells suspension. The samples were respectively taken out after being cultured for 2 and 6 h, washed, and fixed with 2.5% glutaraldehyde for 30 min. After that, the samples were washed with PBS three times, and then was stained by 4′, 6-diamidino-2-phenylindole (DAPI) 5 min for cell counting. Fluorescence microscopy was used to observe the morphology of osteoblast cells, and the actin cytoskeleton was stained by PBS diluted rhodamine. 50 μL diluted rhodamine was dropped onto the surface of samples and was made spreaded out over the whole surface. The process of staining was operated in a darkroom for 15 min; after that, all the stained samples were washed by PBS three times. The number of the samples used for statistical counting was no less than four. A fluorescence microscope was used to obtain 15 random images for statistics of the attached cells.

Osteoblast cell viability was assessed by Cell Counting Kit-8 (CCK-8) after incubation for 1, 3, and 5 days, respectively. The culture medium was removed and the samples were washed three times with PBS. Subsequently, 350 μL of fresh cell culture medium containing 10% CCK-8 reagent was added to each sample and incubated at 37 °C for 2 h in cell culture condition. Afterward, 200 μL of above culture medium was transferred to a 96-well plate and the absorbance was measured at 450 nm by a microplate reader. All the cell viability experiments were performed more than three times.

2.6.3. Alkaline Phosphatase (ALP) Activity Assay. Alkaline phosphatase (ALP) is a hydrolase enzyme responsible for removing phosphate groups from many types of molecules. ALP activity assay

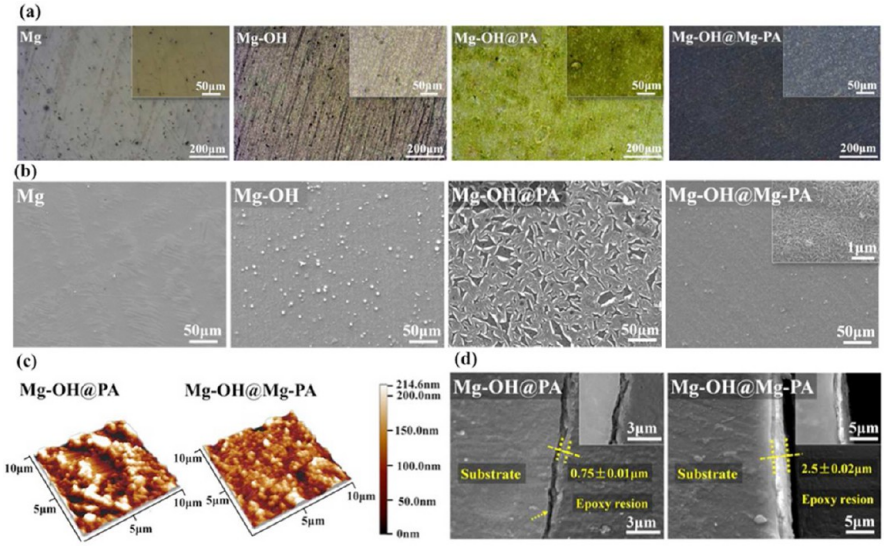

Figure 1. Representative surface morphology of the bare (Mg), alkaline-treated (Mg-OH), direct PA-deposited (Mg-OH@PA) and magnesium ion-integrated PA-deposited (Mg-OH@Mg-PA) Mg: (a) optical images; (b) SEM images; (c) AFM images; (d) cross-section SEM morphology.

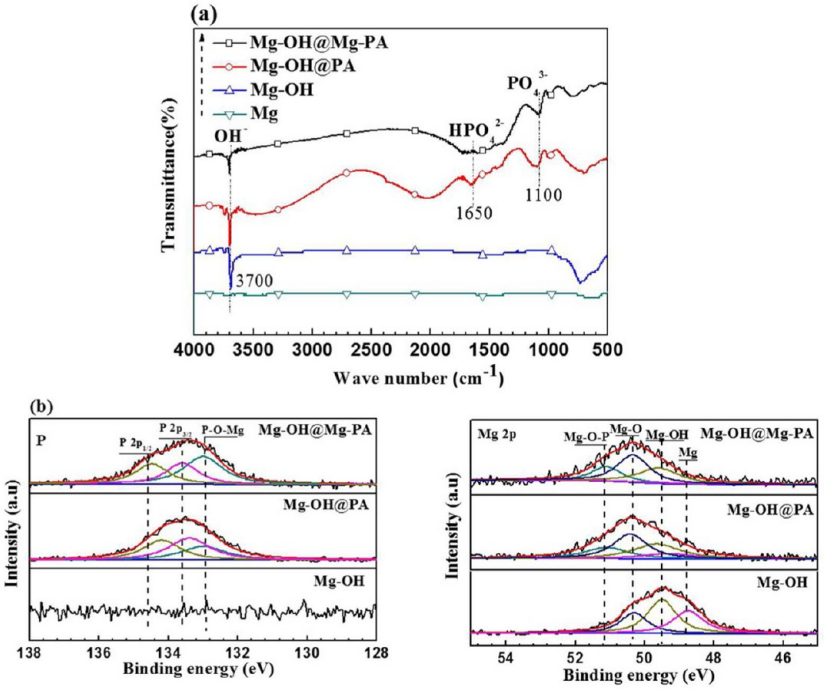

Figure 2. (a) FTIR spectra, and (b) high-resolution XPS P 2p and Mg 2p spectra of the samples surfaces.

measurement offers an effective way to detect the bioactivity of biomaterials pertaining to osteoblast cells' responses of differentiation and mineralization.[43] ALP test was conducted to determine the osteogenic activity of the Mg ion-integrated PA coating up to 21 days (7, 14, and 21 days, respectively). Because of the same limitation above-mentioned for long-term in vitro methodology, the samples were Mg ion-integrated PA coating applied on Ti (Ti-OH@Mg-PA), with the direct PA coated Ti (Ti-OH@PA) and bare Ti for comparison. Briefly, the osteoblast cells were seeded onto samples at a density of 2×10^4 cells/mL. After incubation, the samples were washed with PBS three times and the cells on the samples surface were lysed with 0.4 mL 1% (v/v) Tritan X-100 for 12 h at 4 °C. The cell lysate solution was collected for analysis of total protein level and ALP activity. The total protein concentration of the cell lysate of each sample was measured using the bicinchoninic acid (BCA) protein assay kit. ALP activity was measured using the ALP Assay Kit, and the final ALP activity was normalized with respect to the total protein content obtained from the same cell lysate.[44] The number of the samples used for statistics was no less than four and all the assay was repeated more than two times.

3. RESULTS AND DISCUSSION

3.1. Formation Mechanism of Mg Ion-Integrated PA Layer. Scheme 1 illustrates the formation mechanism of Mg ion-integrated PA coating on the Mg substrate. First, PA molecules are immobilized on the Mg substrate by covalent reaction between their phosphate group ($H\text{-}O_3PO\text{-}R$, myo-inositol-1, 2, 3, 4, 5, 6-hexakisphosphate) and the OH^- group of the $Mg(OH)_2$ layer by means of hydrolysis/neutralization.[34] Subsequently, the Mg with surface-assembled PA were dip-

coated in Mg ions-containing solution to absorb Mg ions. The additive Mg ions do not only promote the chelation reaction with existing PA molecules, but also provide excessive resource ions for chelating with PA molecules of the subsequent dip-coating cycle. An alternating process is thus possible to form a multilayer as a more efficient integrated coating.

3.2. Surface Characterization. For a corrosion-protective coating on magnesium, the efficacy strongly depends on the quality of the film with regards to surface morphology, density and integrity.[45] Figure 1 shows optical microscope (Figure 1a), surface SEM (Figure 1b), AFM (Figure 1c), and cross-section SEM images (Figure 1d) of Mg-OH@Mg-PA as compared with Mg, Mg-OH, and Mg-OH@PA samples. A more uniform coating can be observed on the Mg ion-integrated PA-coated sample (Mg-OH@Mg-PA) as compared with all the other samples (Mg-OH@PA, Mg-OH, and Mg). Note that direct PA-deposited Mg (Mg-OH@PA) presents apparently nonuniform characteristic. SEM images (Figure 1b) confirm further the Mg-OH@Mg-PA sample appears apparently much more homogeneous and denser than all the other samples; the inset amplified SEM image shows a tightly formed whiskerlike phytic acid layer on the Mg surface. This can be attributed to the more efficient PA chelation with magnesium ions. The full and uniform coverage of tightly cross-linked PA coating would help to protect the substrate from corrosion by preventing effectively the electrolyte penetrating into the substrate. In contrast, the direct PA deposited sample (Mg-OH@PA) appears only partly covered by some aggregatelike layers. The aggregated parts are separated with crevicelike space and display some peeling-off at the edges. The AFM images (Figure 1c) confirm a smoother and homogeneous surface morphology on the Mg-OH@Mg-PA sample than on the Mg-OH@PA sample. The cross-section SEM images (Figure 1d) reveal the depth profile of the coating, and the insets were pictured through the backscatter scanning electron microscopic (BSD SEM) which can distinguish magnesium substrate and coating clearly. Accordingly, the Mg-OH@Mg-PA sample acquired a thickness of 2.5 ± 0.02 μm, whereas Mg-OH@PA obtained only 0.75 ± 0.02 μm. Moreover, Mg-OH@Mg-PA presents remarkably a more distinct profile of coating and secure interfacial bonding with Mg substrate as compared with the Mg-OH@PA. The interfacial immobilization was achieved by covalent reaction between chemical conversion $Mg(OH)_2$ passivation layer and PA molecules.[34] The surface morphology as well as cross-sectional observation proves primarily the efficacy of Mg ion chelating with PA molecules to fulfill the deposition of a homogeneous, dense, and thick coating.

To ascertain the magnesium ion-enhanced chelating, we obtained the FT-IR and XPS spectra of the sample surfaces for chemical composition and structure analysis. As shown in Figure 2a, on the surface of the Mg-OH sample there emerged a strong characteristic peak of hydroxyl group (−OH). This indicates that the alkaline pretreatment produced a chemical conversation layer of $Mg(OH)_2$ with large number of hydroxyl groups on the surface of Mg, serving as platform to covalently anchor PA molecules. On the Mg-OH@Mg-PA sample there displays obviously reduced intensity of hydroxyl group peak, suggesting efficient consumption of the hydroxyl group when covalently anchoring the PA molecules on the surface. Both Mg-OH@Mg-PA and Mg-OH@PA present the characteristic peaks of phytic acid at ca. 1100 and 1650 cm^{-1}, identified as $-PO_4^{3-}$ and $-HPO_4^{2-}$, respectively.[34,46] Figure 2b exhibits the high-resolution XPS spectra of P 2p and Mg 2p on the sample surfaces and their deconvolution spectra of bonding states. The surface elemental compositions are listed in Table 1. The

Table 1. Elemental Composition of Samples Surface According to XPS Survey Spectra

samples	C (%)	Mg (%)	O (%)	P (%)
Mg−OH	25.35	22.76	51.89	0
Mg−OH@PA	34.25	10.72	47.69	7.34
Mg−OH@Mg-PA	33.47	12.48	47.11	6.93

appearance of the characteristic phosphorus peak provides the evidence of successful PA deposition, and more Mg elemental composition on Mg-OH@Mg-PA proves the Mg integration.[22] Specifically according to the high resolution XPS spectra and their deconvolution, an obviously stronger proportion of P−O−Mg, identified at ca.132.9 eV, was found on the Mg-OH@Mg-PA than on the Mg-OH@PA. This indicates a higher amount of magnesium ion was integrated into PA coating with the additive Mg ions introduced, and the P−O−Mg provides directly the evidence of the chelation between magnesium ion and PA molecules. The Mg 2p spectra support further the occurrence of Mg chelating with PA molecules as the overall spectra of Mg-OH@Mg-PA and Mg-OH@PA shifted significantly to higher binding energy as compared with Mg-OH samples. Note particularly that a higher amount Mg−O−P bonding state, identified at ca. 51.2 eV, was determined on the Mg-OH@Mg-PA as compared with the Mg-OH@PA sample. This can be ascribed to the extra addition of Mg ions by alternating dipping in Mg ion solution with enhanced chelation. It is worth mentioning that the direct PA deposited samples consume only a low quantity of Mg ions, which are released only from the Mg substrate corrosion.

3.3. Electrochemical Corrosion Behavior. Degradation of biometals is essentially an electrochemical corrosion process which is suitably deciphered by electrochemical testing and analysis.[37] Figure 3 describes the electrochemical potentiodynamic polarization curves and impedance Nyquist spectra of the samples in PBS at 37 ± 0.5 °C. The free corrosion potential E_{corr} and current density i_{corr} were obtained from the polarization curves by Tafel method and the values are listed in Table 2. The Mg-OH@Mg-PA sample underwent the lowest i_{corr} among all the samples and it is significantly smaller than all the other samples, namely nearly 2 orders lower than the pure Mg and 1 order lower than the Mg-OH@PA. Though the Mg-OH@PA has a lower i_{corr} than the Mg-OH, the extent is relatively moderate, implying an insufficient protective effect as compared with the Mg-OH@Mg-PA. The Mg-OH sample shows slightly lower free current density than the bare Mg, suggesting the $Mg(OH)_2$ passivation layer protects the substrate somehow albeit far from satisfactory. The above results indicate that the magnesium ion-integrated PA coating is able to provide a homogeneously complete coverage and a tightly closed barrier of protective layer to prevent Mg corrosion kinetically.

From the electrochemical point of view, the kinetic factors are crucially important for corrosion of the extremely active Mg. The corrosion rate is actually governed by the rate-determining step (RDS) of the overall processes. For phytic acid-coated Mg, the RDS is likely to be the electrolyte diffusion process through the coating unto Mg.[34] A denser and more homogeneous phytic acid layer will provide better corrosion protection by preventing the electrolyte diffusion. Consequently, the sup-

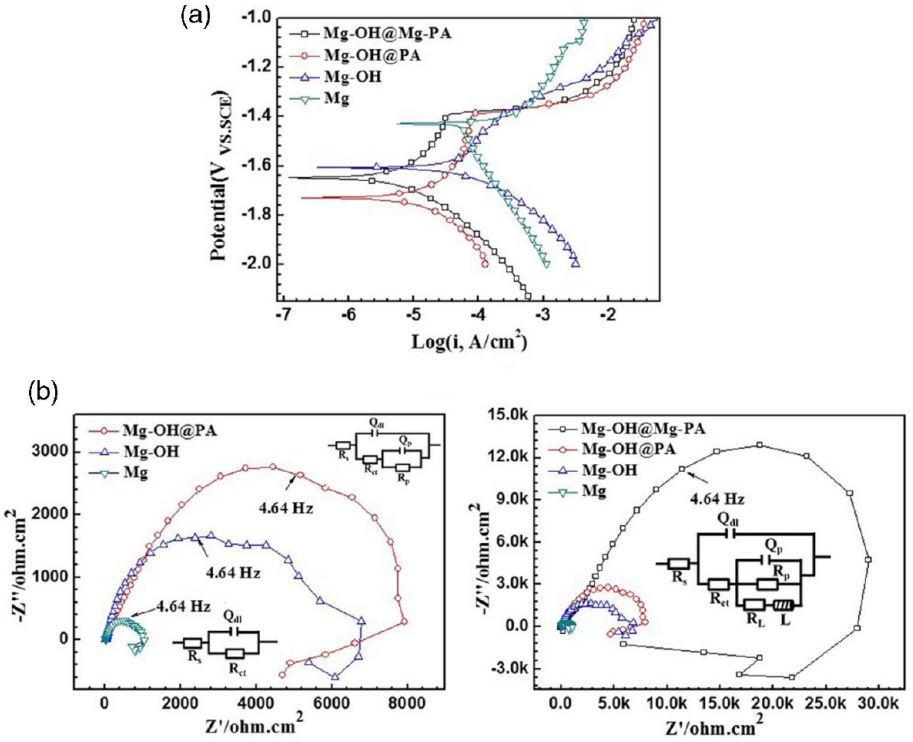

Figure 3. Electrochemical corrosion behavior of the bare (Mg), alkaline-treated (Mg-OH), direct PA-deposited (Mg-OH@PA) and magnesium ion-integrated PA-deposited (Mg-OH@Mg-PA) Mg samples in PBS solution at 37 ± 0.5 °C: (a) potentiodynamic polarization curves; (b) Nyquist EIS spectra.

Table 2. Free Corrosion Potentials E_{corr}, Corrosion Current Densities i_{corr}, and Fitted Results of EIS Spectra of Mg, Mg-OH, Mg-OH@PA, and Mg-OH@Mg-PA in PBS solution at 37 ± 0.5°C

	polarization curves		Nyquist EIS spectra						
samples	$E_{corr}(V_{SCE})$	$\log(i_{corr}$ (A/cm^2))	R_s (Ω cm^2)	R_{ct} (KΩ cm^2)	Q_{dl} (μF cm^2)	R_p (kΩ cm^2)	Q_p (μF cm^2)	R_L (kΩ cm^2)	L (kH cm^2)
Mg	−1.43	−3.75	118	1.38	24.56				
Mg-OH	−1.61	−4.18	125	6.45	27.95	0.11	0.49		
Mg-OH@PA	−1.73	−5.04	129	8.37	15.54	0.14	0.63		
Mg-OH@Mg-PA	−1.64	−5.42	110	32.88	11.12	4.73	0.11	26.66	25.33

pressed electrolyte diffusion RDS results in a reduced corrosion rate. Moreover, the free corrosion potential E_{corr} of coated samples shifted even more negative toward cathodic direction than the bare Mg, this would probably bring down the cathodic hydrogen evolution exchange current density, and therefore partly reduce the overall corrosion rate.[38]

Electrochemical impedance spectroscopy offers a powerful way to fathom the kinetics of electrochemical corrosion of metals. Figure 3b shows the EIS Nyquist spectra of the samples in the PBS solution at 37 ± 0.5 °C. Their corresponding equivalent circuits are embedded in the relevant EIS graph for data fitting and the results are listed in Table 2. The Mg-OH@Mg-PA sample exhibits remarkably overall larger impedance in the entire scanned frequency range than all the other samples. The spectra of coated samples consist of at least two overlapped time constants. The equivalent electrical circuit model of Mg-OH@Mg-PA can be described as $R_s(Q_{dl}(R_{ct}(Q_pR_p(R_L(L)))))$,[47] where R_s represents the solution resistance; Q_{dl} and R_{ct} represent the double layer capacitance and the reaction resistance associated with interfacial charge transfer reaction; Q_p and R_p are related to the coating capacitance and the resistance; and R_L and L represent the inductance resistance and inductance, respectively. Meanwhile, the equivalent electrical circuit of Mg−OH@PA could be described as $R_s(Q_{dl}(R_{ct}(Q_pR_p)))$. In contrast, bare Mg and Mg−OH samples show only one time constant with simplified model $R_s(Q_{dl}R_{ct})$. It is noteworthy that the reaction resistance R_{ct} refers to directly the impedance of the corrosion reaction. The R_{ct} value (Table 2) of Mg-OH@Mg-PA is 30 times and 4 times larger than that of bare Mg and Mg-OH@PA, respectively. Nevertheless, Mg-OH sample possesses slightly larger R_{ct} than bare Mg, implying that the $Mg(OH)_2$ passivation layer have not sufficient corrosion protection ability. The results of EIS Nyquist are consistent with that of the potentiodynamic polarization curves, indicating the corrosion of Mg was inhibited effectively by the Mg ion-integrated PA coating.

3.4. Immersion Degradation Behavior. Because the biocorrosion of Mg-based material evolves dynamically with the kinetic factors wherein, the immersion testing is of practical importance to determine its biodegradation behavior.[37,48] Theoretically, according to the corrosion reaction of magnesium: $Mg + 2H_2O \rightarrow Mg^{2+} + 2OH^- + H_2(g)$, one mole hydrogen produced relates to one mole magnesium corroded.[48,49] Meanwhile, the produced OH^- increases the pH value of the local ambient. Both hydrogen evolution and

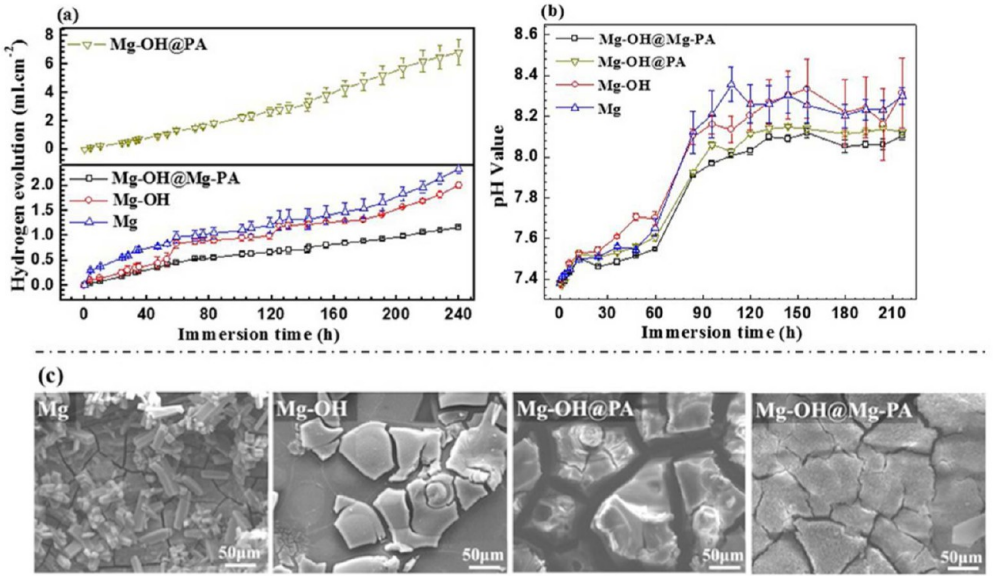

Figure 4. Immersion degradation testing result of the bare (Mg), direct PA deposited (Mg-OH@PA,) and magnesium ion-integrated PA deposited (Mg-OH@Mg-PA) Mg samples in PBS solution at 37 ± 0.5 °C as a function of time: (a) the volume of hydrogen evolved; (b) the pH value of PBS solution; (c) SEM images of the surface morphology of the samples after 240 h immersed in PBS solution (37 ± 0.5 °C).

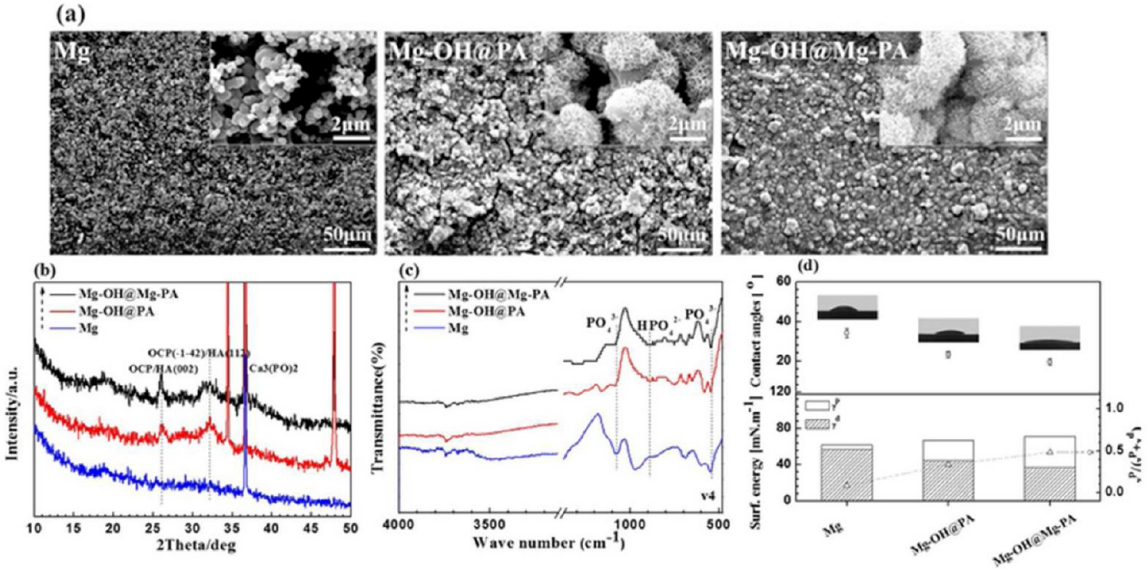

Figure 5. Bioactivity of CaP precipitation on bare Mg, Mg-OH@PA, and Mg-OH@Mg-PA samples: (a) SEM image of surface morphology; (b) XRD patterns; (c) FTIR spectra; (d) Water contact angle and surface energy (γ^p refers to polar part, and γd refers to dispersion part).

increased pH value reflect the Mg corrosion reaction rate indirectly. Figure 4 shows the immersion degradation results of the samples in PBS for 240 h at 37 ± 0.5 °C. It can be found a substantially less quantity of hydrogen evolution as well as increased pH value was gauged on the Mg-OH@Mg-PA than all the other samples during the whole immersion period, and the discrepancy became even larger at late stage. This implies that the Mg ion-integrated PA coating acts as an excellent protective layer to reduce the degradation rate. Note that the Mg-OH@PA produced the highest amount of hydrogen among all the samples particularly at the later stage, suggesting that the nonuniformly aggregated layer accelerates the corrosion of magnesium in the long run. This might be accounted for by the galvanic cells formed adjacent to crevice or local failure which were initiated at early stage. The measured pH value results (Figure 4b) are in agreement with that of the hydrogen evolution, but its variation is not so remarkable might be because of the high aspect ratio of testing solution volume to tested surface area (40 mL/0.79 cm^2) and the pH buffering effect of PBS itself.

In addition, surface SEM observation of the samples after immersion in PBS for 240 h was performed to examine further the degradation behavior. Figure 4c discloses that the Mg-OH@Mg-PA remained still a more intact and uniform coverage of coating as compared with the other samples. The inset images manifest that obvious smaller-size attacks like cracks can be seen on the Mg-OH@Mg-PA compared to the Mg-OH@PA, whereas apparently severer localized corrosion was undergone on the Mg-OH and Mg samples.

dx.doi.org/10.1021/am506741d | ACS Appl. Mater. Interfaces 2014, 6, 19531−19543

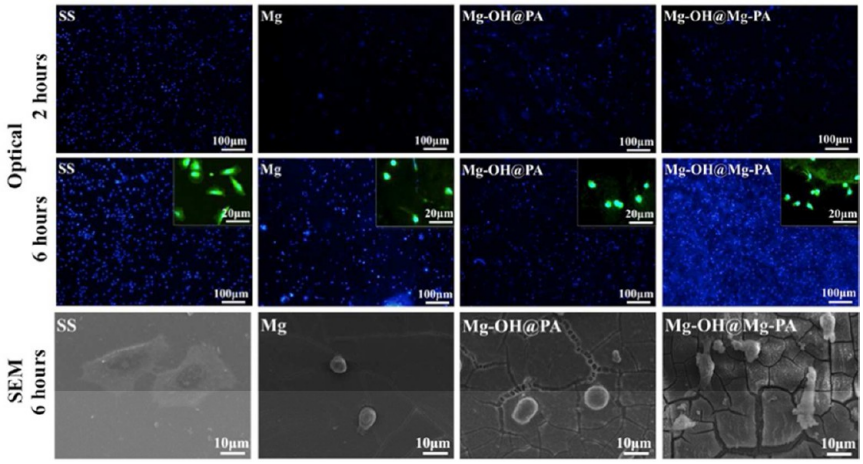

Figure 6. Fluorescence microscopy (cytoskeletal actin (green) and nuclear (blue)) stains of osteoblast and representative SEM images of adherent osteoblast cells on the 316L SS, bare Mg, Mg−OH@PA and Mg−OH@Mg−PA surfaces after 2 and 6 h of culture.

3.5. In Vitro Osteo-Compatibility. *3.5.1. CaP Precipitation.* For an orthopedic biomaterial, in vivo CaP precipitation on the surface is a vital part of the success of biosynthesis and biointegrity of the bone implant.[31] Hereon, in vitro CaP deposition was chosen to judge the bone growth activity of the samples and the results are shown in Figure 5.

Figure 5a shows evidence of the CaP precipitation on the samples surface. On the Mg-OH@Mg-PA and Mg-OH@PA surfaces there developed obviously a thicker layer of CaP as compared to the bare magnesium, and they appeared clearly as a more crystallike structure (the inset images) than on the Mg control. This indicates that the Mg-PA coating essentially promotes the CaP deposition. On one hand, the PA molecules with ultrastrong chelating activity, can capture calcium ions to form a supersaturated calcium phosphate state and provide the nucleation sites for the CaP precipitation; likewise, phosphate groups on the PA molecules mimicking that of bone are likely to support the CaP deposition too. On the other hand, the integrated/chelated Mg ion might enhance further the CaP precipitation through acting as extra nucleation sites similar to the above-mentioned calcium ions. This means Mg ion-integrated PA potentially improves the bioactivity of biodegradable Mg-based materials. More importantly, such more potential nucleation sites would benefit to precipitate a significantly more homogeneous and finer-grained CaP coating, as it was observed on the Mg-OH@Mg-PA surface, compared to the Mg-OH@PA.

X-ray diffraction (XRD) and FTIR analysis were taken to characterize further the phase and chemical structure of the CaP coatings. As shown in XRD spectra (Figure 5b), new characteristic peaks at 26, 32, and 36°, typical for hydroxyapatite ($Ca_{10}(PO_4)_6(OH)_2$, HA) and octacalcium phosphate ($Ca_8H(PO_4)_6{\cdot}5H_2O$, OCP) mimic the bone phases,[27] were detected on the Mg-OH@Mg-PA and Mg-OH@PA samples. It is noteworthy that on the Mg-OH@Mg-PA surface peaks of stronger intensity than on the Mg−OH@PA appeared. In contrast, only the phase of $Ca_3(PO_4)_2$ instead of HA or OCP was identified on the bare Mg sample. Figure 5c depicts the FTIR spectra of the CaP coating on the samples. Accordingly, the CaP precipitated Mg-OH@Mg-PA and Mg-OH@PA samples exhibit typical peaks of the phosphate region (900−1200 cm^{-1}) of HA. The shoulder peak ca. 1075 cm^{-1} corresponds to part of amorphous HA, and the doublet ca. 560 cm^{-1} (centered at 540 and 580 cm^{-1}, respectively) relates to the PO_4^{3-} v4 bending frequency of HA or OCP, both of which were checked out on the CaP precipitated Mg-OH@PA and Mg-OH@Mg-PA surfaces,[50] but it is more remarkable on the latter. The chemical structure results support the improved CaP precipitation of Mg ion-integrated PA coating.

Beyond chemical characteristics, the physiochemical state like hydrophilicity of surface plays an important role in the bioactivity of biomaterials too. Figure 5d elucidates measured water contact angle, calculated surface energy as well as its polar and dispersion contributions. The Mg-OH@PA and Mg-OH@Mg-PA have water contact angle values of 23.3 and 19.5°, respectively, apparently lower than that of Mg (34.2°). This means the PA coating renders the surface more hydrophilic. The increased hydrophilicity can be unveiled by surface energy calculation that the polar part ratio of the Mg-OH@Mg-PA is distinctly larger than that of Mg-OH@PA and Mg. This is perhaps due to more effectively anchored PA molecule, which is rich in hydrophilic hydroxyl groups. The larger polar surface energy accounts partly for the tendency of CaP precipitation because of electrostatic interactions.[51]

3.5.2. Short-Time in Vitro Osteoblast Adherence and Morphology. Osteoblasts' proper response to orthopedic biomaterial is another important aspect of osto-compatibility, predicting directly the osteo-conductive and -inductive functions of material and therefore the fate of the implant.[40] Figure 6 describes the representative osteoblast adhesion counting and morphology observation of the samples. 316L stainless steel (SS), as widely used orthopedic material, was added as an additional control. The stained cells adherent on samples surface were analyzed by fluorescent microscopy; images are superposed for cytoskeletal actin (green) and nuclear (blue) staining to reassure the existence of osteoblast cells. The number of cells is clearly larger on Mg-OH@Mg-PA surface both after 2 and 6 h culture as compared with Mg and Mg-OH@PA. The number of cells is clearly larger on Mg-OH@Mg-PA surface both after 2 and 6 h culture as compared with Mg and Mg-OH@PA. Although on Mg-OH@Mg-PA adhered slightly less cells than on 316L SS after 2h culture, it induced evidently larger number of cells than the 316L SS after 6h culture. This manifests Mg-OH@Mg-PA performed more osteogenic than the stainless steel and other samples. The inset fluorescence microscopy and SEM morphology illustrate that

the cells on the Mg-OH@Mg-PA appear more elongated than the cells on the SS, Mg and Mg-OH@PA, providing the evidence for the increased proliferation of osteoblast cells. Note that the cells on SS appeared bigger with more spreading extent; this conformal change reflects a less natural state than cells on the Mg-OH@Mg-PA sample. Figure 7 provides the

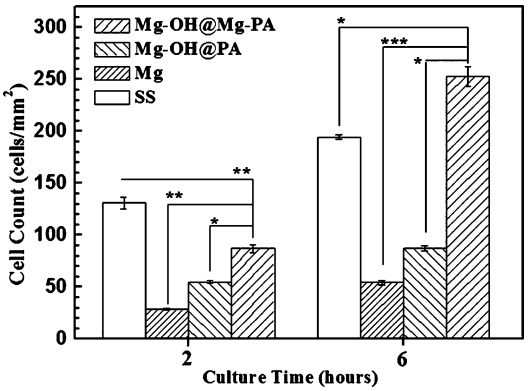

Figure 7. Statistical counting of osteoblast cells adherent onto the 316L SS, bare Mg, Mg−OH@PA and Mg−OH@Mg−PA surfaces after 2 and 6 h culture. Data presented as mean ± SD and analyzed using a ANOVA, *p < 0.05, **p < 0.01, ***p < 0.001.

statistical analysis results; particularly the cell density on the Mg−OH@Mg-PA surface is remarkably larger than that on SS. The ligandlike chelated product between magnesium ion and PA with more bone-mimetic properties might be beneficial for recruiting osteoblast cells and supporting their proliferation.[52]

Considering real in vivo circumstance, we assessed further the CaP precipitated samples regarding osteoblast behavior. In fact, bioactive bone-growth and cell expression will occur and interact always simultaneously on a biomaterials surface in clinical practice. Figure 8 portrays the fluorescence microscopy and representative SEM images of osteoblast cells on the CaP precipitated samples and Figure 9 displays the statistical counting of osteoblasts adherent on the CaP precipitated samples. As the cell culture was conducted in parallel and with

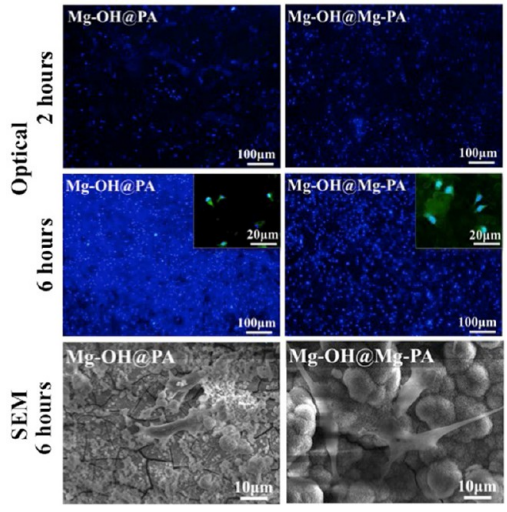

Figure 8. Fluorescence microscopy (cytoskeletal actin (green) and nuclear (blue)) stains of osteoblast and representative SEM images of adherent osteoblast cells on CaP deposited Mg-OH@PA and Mg-OH@Mg-PA surfaces after 2 and 6 h of culture.

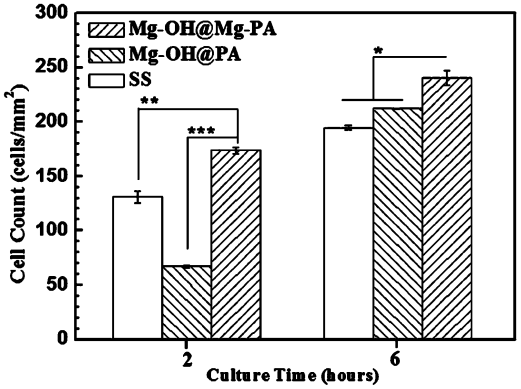

Figure 9. Statistical counting of osteoblast cells adherent onto the CaP deposited Mg-OH@PA and Mg-OH@Mg-PA surfaces as compared with SS surfaces after 2 and 6 h of culture. Data presented as mean ± SD and analyzed using an ANOVA, *p < 0.05, **p < 0.01, ***p < 0.001.

same condition as for the above results (Figure 6 and Figure 7), the data can be compared directly. After 2 and 6 h culture, apparently more osteoblast cells adhered on the CaP precipitated Mg-OH@Mg-PA sample than on the CaP precipitated Mg-OH@PA sample. It is worth noting that more cells on the CaP precipitated Mg-OH@PA can be observed than on its counterpart without CaP deposition. The density of cells on the CaP precipitated Mg-OH@Mg-PA are higher than both the SS and Mg-OH@PA for 2 and 6 h culture, whereas on the Mg-OH@PA there adhered less cells than SS for 2 h culture but this became reversed after 6 h culture. Further, SEM images of osteoblasts on the CaP precipitated samples demonstrate remarkably the stronger signs of cells proliferation, i.e., protrusions extending along surface, as compared with unprecipitated samples. Noticeably, a distinct cytoplasm spreading state preferentially along the CaP crystals can be recognized on the CaP-precipitated Mg-OH@Mg-PA, supposing a more naturally active and proliferative fate of the cells; while the rounder state of the cells on the other samples presumes a tendency of premature death. The short-time in vitro results envisage our Mg ion-integrated PA-coated Mg might fulfill a potentially osteo-integrative, -conductive, and -inductive biofunctionality.[51,52]

3.5.3. Long-Time in Vitro Osteoblast Adhesion and Viability. Current long-term in vitro methodology for cytocompatibility is not applicable for magnesium-based specimens, due to the relatively high corrosion rate which changes the cell culture medium dramatically,[53] namely, the released magnesium ion, hydrogen evolution and change of pH value influence the accuracy of analytical methods (for example, staining). This situation goes also beyond the real in vivo condition for cells' adhesion, spreading and differentiation.[54] For coatings, one alterative is to examine their cytocompatibility on a more inert substrate indirectly.[54,55] In our case, osteoblast cells were cultured on a Mg-PA coating on a Ti surface for longer-time evaluation pertaining to osteoblast viability, differentiation and mineralization.

Figure 10 presents the representative osteoblasts adherent on the Ti-OH@Mg-PA, Ti-OH@PA and Ti sample surfaces up to 5 days. Optical fluorescence microscopy observation shows that the number of cells is clearly larger on the Ti-OH@Mg-PA surface both for 1, 3, and 5 days culture as compared with Ti-OH@PA, and nearly the same to the bare Ti. Meanwhile, the

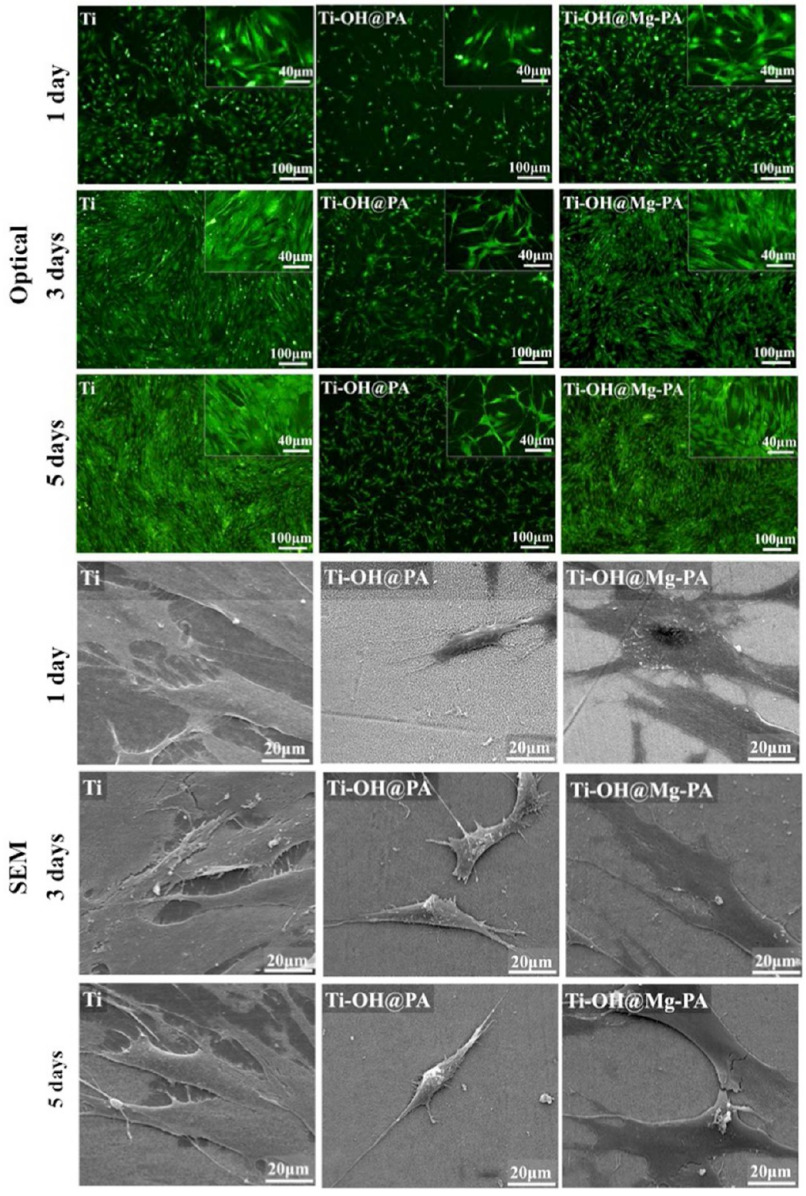

Figure 10. Fluorescence microscopy (cytoskeletal actin (green)) stains of osteoblast and representative SEM images of adherent osteoblast cells on the Ti-OH@Mg-PA, Ti-OH@PA, and Ti surfaces after 1, 3, and 5 days of culture.

SEM observation illustrates that the cells on Ti-OH@Mg-PA surface exhibit a more natural spreading state with pseudopodia and fusiform- morphology,[56] in contrast to those on Ti-OH@PA which appear round and at less spreading state. Both the number and morphology of the cells on the Ti−OH@Mg-PA surface are comparable to those on bare Ti. Figure 11 provides the cell viability (CCK-8) results of the Ti-OH@Mg-PA in comparison to Ti−OH@PA and Ti samples. There is significantly larger number of viable cells can be detected on the Ti-OH@Mg-PA surface as compared with Ti-OH@PA surface. Particularly, the difference became increasingly significant with the testing time increasing from 1, 3 to 5 days. The cells viability on the Ti-OH@Mg-PA surface is still comparable to that of the Ti surface. Combining the cells adhesion and viability results, we deduce that the Mg ion integration could improve apparently the PA coating's osteogenic performance in terms of cell proliferation and viability, to a level comparable with pure Ti, which is one of the most biocompatible metals clinically used.

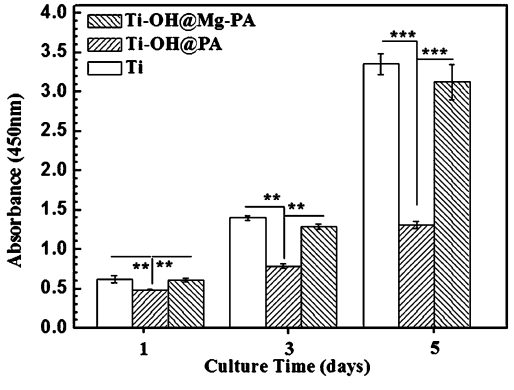

Figure 11. Osteoblast cell viability (cell counting Kit-8, CCK8) on the Ti-OH@Mg-PA, Ti-OH@PA, and Ti surface after 1, 3, and 5 days of culture. Data presented as mean ± SD and analyzed using an ANOVA, $^{**}p < 0.01$, $^{***}p < 0.001$.

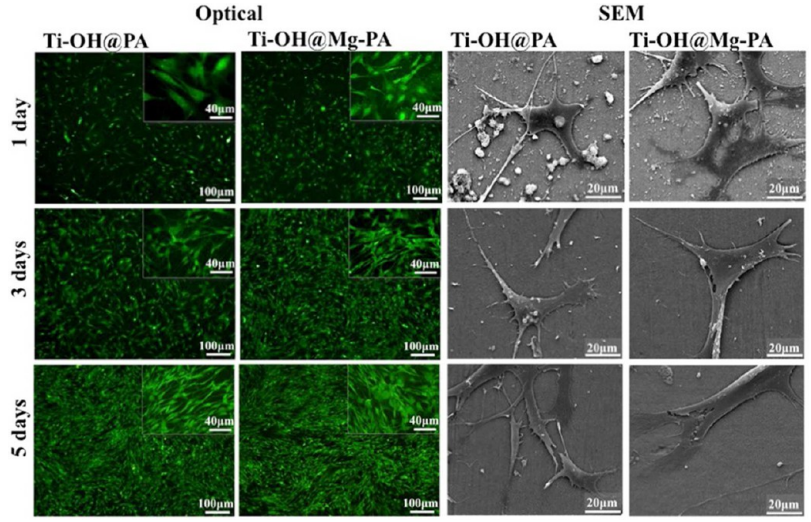

Figure 12. Fluorescence microscopy (cytoskeletal actin (green)) stains of osteoblast and representative SEM images of adherent osteoblast cells on CaP deposited Ti−OH@PA and Ti−OH@Mg−PA surfaces after 1, 3, and 5 days of culture.

Similar to the short-time evaluation, CaP-precipitated samples of Ti-OH@Mg-PA and Ti-OH@PA were also further checked concerning their osteogenic behavior. Figure 12 displays the fluorescence and SEM images of osteoblast cells on the Mg-PA coated Ti after CaP precipitation as compared with the direct PA-coated Ti. Identically, the cell culture was conducted in parallel and at the same conditions as the above results (Figures 10 and 11), and they can be compared directly. Interestingly, on the Ti substrate there seems to no significant difference between the CaP precipitated Ti-OH@Mg-PA and Ti-OH@PA samples, what is in contrast to the short-time results on the Mg substrate (Figure 8). This manifests the Mg ions released from Mg corrosion/degradation probably play a positive role in promoting the bioactive of CaP precipitation and osteoblasts responses.[55] This favors for the application of such coating on the Mg substrate. Furthermore, Figure 13 reveals the cell viability results (CCK-8) of the CaP precipitated samples of Ti-OH@Mg-PA and Ti-OH@PA. There was no obvious difference between both CaP-precipitated samples, albeit they presented slightly lower values than bare Ti. This might be ascribed to the shielding effect of the predeposited CaP layer on the Mg-ion integrated PA surface, which in turn implies the Mg-ion integration per se plays a critical role in the better osteogenicity of the Mg-ion integrated PA coating.

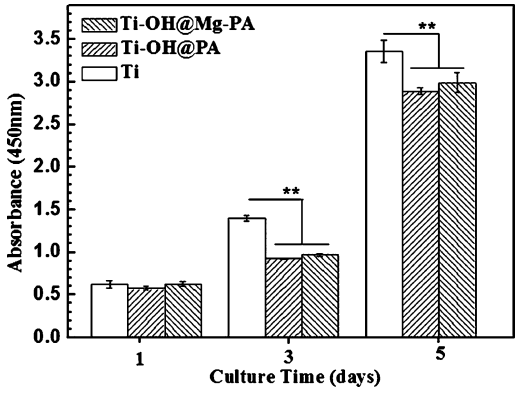

Figure 13. Osteoblast cell viability (cell counting Kit-8, CCK8) on the CaP-deposited Ti−OH@PA and Ti−OH@Mg−PA surfaces as compared with Ti surface after 1, 3, and 5 days of culture. Data presented as mean ± SD and analyzed using an ANOVA, $^{**}p < 0.05$.

3.5.4. Alkaline Phosphatase (ALP) Activity. ALP activity is a commonly used indicator of osteoblast cell differentiation on biomaterials surface.[43,44] Figure 14 presents the ALP results of

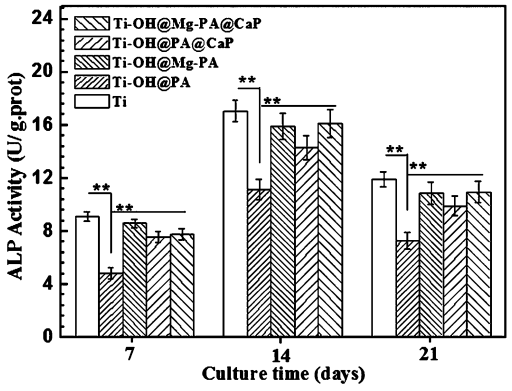

Figure 14. Alkaline phosphatase (ALP) activity of osteoblasts on Ti, Ti-OH@PA, and Ti-OH@Mg-PA and CaP deposited samples of Ti-OH@PA@CaP and Ti-OH@Mg-PA@CaP surfaces after 7, 14, and 21 days of culture. Data presented as mean ± SD and analyzed using an ANOVA, $^{**}p < 0.01$.

all the samples described above. As shown, the Ti-OH@Mg-PA sample induced significant better differentiation as compared with Ti-OH@PA sample for 7, 14, and 21 days culture, which is slightly lower albeit still comparable to Ti. For the CaP precipitated Ti-OH@PA samples, it behaved better than its counterpart without precipitation in the cells differentiation, but obviously less than both the CaP precipitated Ti-OH@Mg-PA and its counterpart of no precipitation. For Ti-OH@Mg-PA, the CaP precipitated sample perform less osteogenic than its counterpart at earlier 7 days, whereas it improved and became comparable to its counterpart at 14 and 21 days. This maybe explained by the integrated Mg ions being more exposed or released at late stage, which needs to be studied further. In short, the above ALP results purport that the Mg ion integration enhances the PA coating's osteoblastic differ-

entiation, and the level can be comparable to that of pure Ti as the standard choice in current clinical practice.

To sum up its dual-task performance of corrosion-control and osteo-compatibility, we ascertain that our Mg ion-integrated PA coating accomplishes an improved coating integrity and therefore better-controlled biocorrosion/degradation rate, and more importantly the nature of the Mg ions as well as PA molecules would endow the coating with enhanced osteogenic biofunctionality. Note the limitation of current in vitro methodology makes the long-term performance still unclear for the real coating on the targeted Mg metal substrate.[41,53−55] Nonetheless, the results on Ti disclose at least partly the feature and mechanism of osteogenicity performed by the coating per se. The point is it reportedly seems unlikely that the Mg ions released by corrosion/degradation will do harm to the osteo-compatibility;[57,58] in contrast, there is more chance that they might pose benign effects on the bone responses. Nevertheless, the future work should fathom more the interactions thereof and move forward to in vivo evaluations in the end.

4. CONCLUSIONS

A magnesium ion-integrated phytic acid coating was covalently constructed on pure magnesium by employing a combination of chemical conversion and alternated dip-coating approaches. The coating was designed to fulfill clinically oriented dual-task performance of biodegradation-control and osteo-compatibility. The obtained coating accomplished an excellent protection on biocorrosion in phosphate buffered saline and therefore in vitro biodegradation of magnesium. The protective efficacy is attributed to the improved coating quality, namely better homogeneity, higher density and thickness, brought about from Mg ion-enhanced phytic acid deposition. Distinguishingly, the nature of magnesium ion-integrated PA coating renders the surface potentially osteo-compatible. The bioactive surface promotes CaP precipitation to prompt osteo-integrative performance, and induces osteoblast cells to adhere and proliferate so as to support osteo-conductive and -inductive biofunctionality. Thus, our prepared ligand-like Mg ion-integrated PA modified Mg bodes promisingly for the biodegradable application of bone implants.

AUTHOR INFORMATION

Corresponding Author

*E-mail: guojiang.wan@home.swjtu.edu.cn, superwgj@263.net, or guojiang.wan@googlemail.com. Tel: +86 28 8763 4146, ext. 802. Fax: +86 28 8760 0625.

Notes

The authors declare no competing financial interest.

ACKNOWLEDGMENTS

We gratefully thank Dr. Manfred F. Maitz of Leibniz Institute of Polymer Research Dresden (Germany) for his language revision and technical discussion. This work was financially supported by the National Natural Science Foundation of China under Grant (21473138, 20973134, and 81330031), Key Basic Research Program of China (2011CB606204), Sichuan Youth Science & Technology Foundation (2012JQ0001) for Distinguished Young Scholars.

REFERENCES

(1) Bauer, S.; Schmuki, P.; Mark, K.; Park, J. Engineering Biocompatible Implant Surfaces Part I: Materials and Surfaces. *Prog. Mater. Sci.* **2013**, *58*, 261−326.
(2) Niinomi, M.; Nakai, M.; Hieda, J. Development of New Metallic Alloys for Biomedical Application. *Acta Biomater.* **2012**, *8*, 3888−3903.
(3) Zberg, B.; Uggowitzer, P. J.; Löffler, J. F. MgZnCa Glasses without Clinically Observable Hydrogen Evolution for Biodegradable Implants. *Nat. Mater.* **2009**, *8*, 887−891.
(4) Staiger, M. P.; Pietak, A. M.; Huadmai, J.; Dias, G. Magnesium and Its Alloys as Orthopedic Biomaterials: A Review. *Biomaterials* **2006**, *27*, 1728−1734.
(5) Mani, G.; Feldman, M. D.; Patel, D.; Agrawal, C. M. Coronary Stents: A Materials Perspective. *Biomaterials* **2007**, *28*, 1689−1710.
(6) Nair, L. S.; Laurencin, C. T. Biodegradable Polymers as Biomaterials. *Prog. Polym. Sci.* **2007**, *32*, 762−798.
(7) Wu, G.; Ibrahim, J. M.; Chu, P. K. Surface Design of Biodegradable Magnesium Alloys - A Review. *Surf. Coat. Technol.* **2013**, *233*, 2−12.
(8) Witte, F.; Fischer, J.; Nellesen, J.; Crostack, H. A.; Kaese, V.; Pisch, A.; Beckmann, F.; Windhagen, H. In Vitro and in Vivo Corrosion Measurements of Magnesium Alloys. *Biomaterials* **2006**, *27*, 1013−1018.
(9) Zeng, R.; Dietzel, W.; Witte, F.; Hort, N.; Blawert, C. Progress and Challenge for Magnesium Alloys as Biomaterials. *Adv. Eng. Mater.* **2008**, *10*, B3−B14.
(10) Narayanan, T. S.; Park, I. S.; Lee, M. H. Strategies to Improve the Corrosion Resistance of Microarc Oxidation (MAO) Coated Magnesium Alloys for Degradable Implants: Prospects and Challenges. *Prog. Mater. Sci.* **2014**, *60*, 1−71.
(11) Witte, F. The History of Biodegradable Magnesium Implants: A Review. *Acta Biomater.* **2010**, *6*, 1680−1692.
(12) Kirkland, N. T.; Lespagnol, J.; Birbilis, N.; Staiger, M. P. A Survey of Bio-corrosion Rates of Magnesium Alloys. *Corros. Sci.* **2010**, *52*, 287−291.
(13) Song, G. Control of Biodegradation of Biocompatible Magnesium Alloys. *Corros. Sci.* **2007**, *49*, 1696−1701.
(14) Xin, Y.; Hu, T.; Chu, P. K. In Vitro Studies of Biomedical Magnesium Alloys in a Simulated Physiological Environment: A Review. *Acta Biomater.* **2011**, *7*, 1452−1459.
(15) Mao, L.; Yuan, G.; Wang, S.; Niu, J.; Wu, G.; Ding, W. A Novel Biodegradable Mg-Nd-Zn-Zr alloy with Uniform Corrosion Behavior in Artificial Plasma. *Mater. Lett.* **2012**, *88*, 1−4.
(16) Kannan, M. B.; Raman, R. K. S. In Vitro Degradation and Mechanical Integrity of Calcium-containing Magnesium Alloys in Modified-simulated Body Fluid. *Biomaterials* **2008**, *29*, 2306−2314.
(17) Bornapour, M.; Muja, N.; Shum-Tim, D.; Cerruti, M.; Pekguleryuz, M. Biocompatibility and Biodegradability of Mg-Sr alloys: The Formation of Sr-substituted Hydroxyapatite. *Acta Biomater.* **2013**, *9*, 5319−5330.
(18) Park, R. S.; Kim, Y. K.; Lee, S. J.; Jang, Y. S.; Park, S.; Yun, Y. H.; Bae, T. S.; Lee, M. H. Corrosion Behavior and Cytotoxicity of Mg-35Zn-3Ca Alloy for Surface Modified Biodegradable Implant Material. *J. Biomed. Mater. Res., Part B* **2012**, *100*, 911−923.
(19) Gray, J. E.; Luan, B. Protective Coatings on Magnesium and Its Alloys - A Critical Review. *J. Alloys Compd.* **2002**, *336*, 88−113.
(20) Wan, G. J.; Maitz, M. F.; Sun, H.; Li, P. P.; Huang, N. Corrosion Properties of Oxygen Plasma Immersion Ion Implantation Treated Magnesium. *Surf. Coat. Technol.* **2007**, *201*, 8267−8272.
(21) Wu, X.; Su, P.; Jiang, Z.; Meng, S. Influences of Current Density on Triblogical Characteristics of Ceramic Coatings on ZK60 Mg Alloy by Plasma Electrolytic Oxidation. *ACS Appl. Mater. Interfaces* **2010**, *2*, 808−812.
(22) Ishizaki, T.; Okido, M.; Masuda, Y.; Saito, N.; Sakamoto, M. Corrosion Resistant Performances of Alkanoic and Phosphonic Acids Derived Self-Assembled Monolayers on Magnesium Alloy AZ31 by Vapor Phase Method. *Langmuir* **2011**, *27*, 6009−6017.

(23) Gu, X. N.; Zheng, W.; Cheng, Y.; Zheng, Y. F. A Study on Alkaline Heat Treated Mg-Ca alloy for the Control of the Biocorrosion Rate. *Acta Biomater.* **2009**, *5*, 2790−2799.
(24) Liang, J.; Hu, L.; Hao, J. Improvement of Corrosion Properties of Microarc Oxidation Coating on Magnesium Alloy by Optimizing Current Density Parameters. *Appl. Surf. Sci.* **2007**, *253*, 6939−6945.
(25) Blawert, C.; Dietzel, W.; Ghali, E.; Song, G. Anodizing Treatment for Magnesium Alloys and Their Effect on Corrosion Resistance in Various Environments. *Adv. Eng. Mater.* **2006**, *8*, 511−533.
(26) Zhang, X.; Li, X. W.; Li, J. G.; Sun, X. D. Preparation and Characterizations of Bioglass Ceramic Cement/Ca-P Coating on Pure Magnesium for Biomedical Applications. *ACS Appl. Mater. Interfaces* **2014**, *6*, 513−525.
(27) Wong, H. M.; Yeung, K. W. K.; Lam, K. O.; Tam, V.; Chu, P. K.; Luk, K. D. K.; Cheung, K. M. C. A Biodegradable Polymer-based Coating to Control the Performance of Magnesium Alloy Orthopaedic Implants. *Biomaterials* **2010**, *31*, 2084−2096.
(28) Wang, J.; He, Y.; Maitz, M. F.; Collins, B.; Xiong, K. Q.; Guo, L.; Yun, Y.; Wan, G.; Hang, N. A Surface-eroding poly(1,3-trimethylene carbonate) Coating for Fully Biodegradable Magnesium-based Stent Applications: Toward Better Biofunction, Biodegradation and Biocompatibility. *Acta Biomater.* **2013**, *9*, 8678−8689.
(29) Wang, J.; Tang, J.; Zhang, P.; Li, Y.; Wang, J.; Lai, Y.; Qin, L. Surface Modification of Magnesium Alloys Developed for Bioabsorbable Orthopedic Implants: A General Review. *J. Biomed. Mater. Res., Part B* **2012**, *100*, 1691−1701.
(30) Xu, W.; Song, J.; Sun, J.; Lu, Y.; Yu, Z. Rapid Fabrication of Large-Area, Corrosion-Resistant Superhydrophobic Mg Alloy Surfaces. *ACS Appl. Mater. Interfaces* **2011**, *3*, 4404−4414.
(31) Shadanbaz, S.; Dias, G. J. Calcium Phosphate Coatings on Magnesium Alloys for Biomedical Applications: A Review. *Acta Biomater.* **2012**, *8*, 20−30.
(32) Cheryan, M.; Rackis, J. J. Phytic Acid Interaction in Food Systems. *Crit. Rev. Food Sci. Nutr.* **1980**, *13*, 279−335.
(33) Johnson, L. F.; Tate, M. E. Structure of "Phytic Acids. *Can. J. Chem.* **1969**, *47*, 63−73.
(34) Chen, Y.; Wan, G.; Wang, J.; Zhao, S.; Zhao, Y.; Huang, N. Covalent Immobilization of Phytic Acid on Mg by Alkaline Pretreatment: Corrosion and Degradation Behavior in Phosphate Buffered Saline. *Corros. Sci.* **2013**, *75*, 280−286.
(35) Liang, C. H.; Zheng, R. F. Conversion Coating Treatment for AZ91 Magnesium Alloys by a Permanganate-REMS. *Mater. Corros.* **2007**, *58*, 193−197.
(36) Owens, D. K.; Wendt, R. C. Estimation of the Surface Free Energy of Polymers. *J. Appl. Polym. Sci.* **1969**, *13*, 1741−1747.
(37) Shi, Z.; Liu, M.; Atrens, A. Measurement of the Corrosion Rate of Magnesium Alloys Using Tafel Extrapolation. *Corros. Sci.* **2010**, *52*, 579−588.
(38) Frankel, G. S.; Samaniego, A.; Birbilis, N. Evolution of Hydrogen at Dissolving Magnesium Surfaces. *Corros. Sci.* **2013**, *70*, 104−111.
(39) Miyazaki, T.; Kim, H. M.; Miyaji, F.; Kokubo, T.; Kato, H.; Nakamura, T. Bioactive Tantalum Metal Prepared by NaOH Treatment. *J. Biomed. Mater. Res.* **2000**, *50*, 35−42.
(40) Zomorodian, A.; Garcia, M. P.; Silva, T.; Fernandes, J.; Fernandes, M.; Montemor, M. Corrosion Resistance of a Composite Polymeric Coating Applied on Biodegradable AZ31 Magnesium Alloy. *Acta Biomater.* **2013**, *9*, 8660−8670.
(41) Zhang, S.; Li, J.; Song, Y.; Zhao, C.; Zhang, X.; Xie, C.; Zhang, Y.; Tao, H.; He, Y.; Jiang, Y.; Bian, Y. In Vitro Degradation, Hemolysis and MC3T3-E1 Cell Adhesion of Biodegradable Mg-Zn alloy. *Mater. Sci. Eng., C* **2009**, *29*, 1907−1912.
(42) Hu, Y.; Cai, K.; Luo, Z.; D.Jandt, K. Layer-by-layer Assembly of β-estradiol Loaded Mesoporous Silica Nanoparticles on Titanium Substrates and Its Implication for Bone Homeostasis. *Adv. Mater.* **2010**, *22*, 4146−4150.
(43) Guicheux, J.; Lemonnier, J.; Ghayor, C.; Suzuki, A.; Palmer, G.; Caverzasio, J. Activation of p38 Mitogen-activated Protein Kinase and c-Jun-NH2-terminal Kinase by BMP-2 and Their Implication in the Stimulation of Osteoblastic Cell Differentiation. *J. Bone Miner. Res.* **2003**, *18*, 2060−2068.
(44) Wang, Z.; Wang, K.; Lu, X.; Li, M.; Liu, H.; Xie, C.; Meng, F.; Jiang, O.; Li, C.; Zhi, W. BMP-2 Encapsulated Polysaccharide Nanoparticle Modified Biphasic Calcium Phosphate Scaffolds for Bone Tissue Regeneration. *J. Biomed. Mater. Res., Part A* **2014**, DOI: 10.1002/jbm.a.35282.
(45) Hornberger, H.; Virtanen, S.; Boccaccini, A. R. Biomedical Coatings on Magnesium Alloys - A Review. *Acta. Biomater.* **2012**, *8*, 2442−2455.
(46) Cui, X.; Li, Q.; Li, Y.; Wang, F.; Jin, G.; Ding, M. Microstructure and Corrosion Resistance of Phytic Acid Conversion Coatings for Magnesium Alloy. *Appl. Surf. Sci.* **2008**, *255*, 2098−2103.
(47) Ye, C. H.; Zheng, Y. F.; Wang, S. Q.; Xi, T. F.; Li, Y. D. In Vitro Corrosion and Biocompatibility Study of Phytic Acid Modified WE43 Magnesium Alloy. *Appl. Surf. Sci.* **2012**, *258*, 3420−3427.
(48) Kirkland, N. T.; Birbilis, N.; Staiger, M. P. Assessing the Corrosion of Biodegradable Magnesium Implants: A Critical Review of Current Methodologies and Their Limitations. *Acta Biomater.* **2012**, *8*, 925−936.
(49) Song, G. Recent Progress in Corrosion and Protection of Magnesium Alloys. *Adv. Eng. Mater.* **2005**, *7*, 563−586.
(50) Chang, M. C.; Tanaka, J. FT-IR Study for Hydroxyapatite/collagen Nanocomposite Cross-linked by Glutaraldehyde. *Biomaterials* **2002**, *23*, 4811−4818.
(51) Oyane, A.; Wang, X.; Sogo, Y.; Ito, A.; Tsurushima, H. Calcium Phosphate Composite Layers for Surface-mediated Gene Transfer. *Acta Biomater.* **2012**, *8*, 2034−2046.
(52) Samavedi, S.; Whittington, A. R.; Goldstein, A. S. Calcium Phosphate Ceramics in Bone Tissue Engineering: A review of Properties and Their Influence on Cell Behavior. *Acta Biomater.* **2013**, *9*, 8037−8045.
(53) Gu, X.; Zheng, Y.; Zhong, S.; Xi, T.; Wang, J.; Wang, W. Corrosion of, and Cellular Response to Mg-Zn-Ca Bulk Metallic Glasses. *Biomaterials* **2010**, *31*, 1093−1103.
(54) Zhao, Y.; Jamesh, M.; Li, W.; Wu, G.; Wang, C.; Zheng, Y.; Yeung, K.; Chu, P. Enhanced Antimicrobial Properties, Cytocompatibility, and Corrosion Resistance of Plasma-modified Biodegradable Magnesium Alloys. *Acta Biomater.* **2014**, *10*, 544−556.
(55) Walker, J.; Shadanbaz, S.; Woodfied, T.; Staiger, M.; Dias, G. Magnesium Biomaterials for Orthopedic Application: A Review from a Biological Perspective. *J. Biomed. Mater. Res., Part B* **2014**, *102*, 1316−1331.
(56) Guehennec, L.; Lopez-Heredia, M.; Enkel, B.; Weiss, P.; Amouriq, Y.; Loyrolle, P. Osteoblastic Cell Behavior on Different Titanium Implant Surface. *Acta Biomater.* **2008**, *4*, 535−543.
(57) Yoshizawa, S.; Brown, A.; Barchowsky, A.; Sfeir, C. Magnesium Ion Stimulation of Bone Marrow Stromal Cells Enhances Osteogenic Activity, Simulating the Effect of Magnesium Alloy Degradation. *Acta Biomater.* **2014**, *10*, 2834−2842.
(58) Witte, F.; Kaese, V.; Haferkamp, H.; Switzer, E.; Meyer-Lindenberg, A.; Wirth, C. J.; Windhagena, H. In Vivo Corrosion of Four Magnesium Alloys and the Associated Bone Response. *Biomaterials* **2005**, *26*, 3557−3563.